Far-Field Drag Computation and the Influence of Wake Modeling

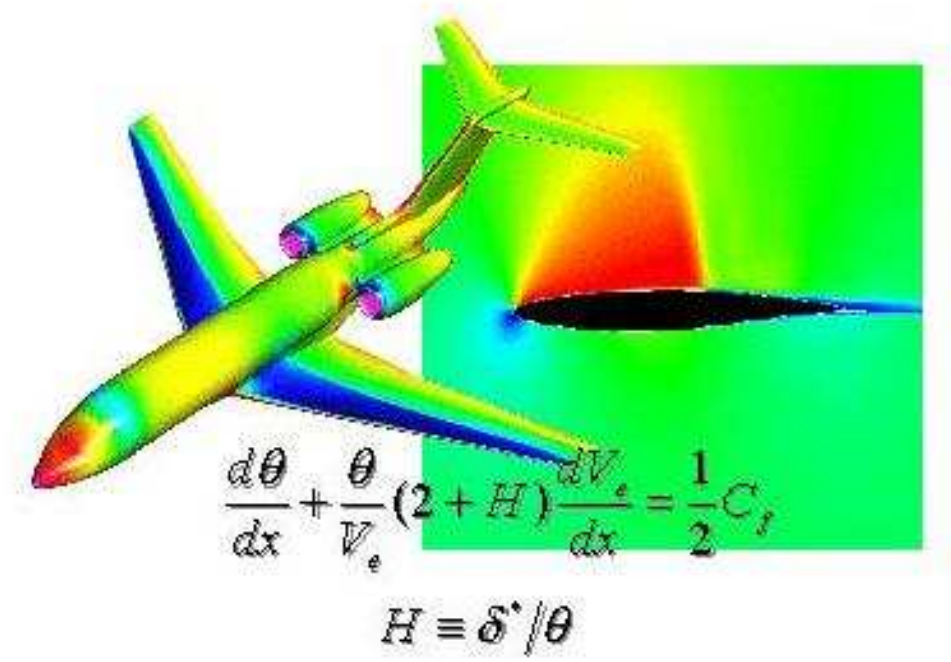

AA200b

Lecture 15-16

February 23-24, 2005

Far-Field Drag Computation

There is a substantial amount of evidence that the accuracy of surface pressure integration is insufficient for a careful study of induced drag and therefore alternate techniques are required. This is particularly due to the fact that in typical wing configurations, the computation of induced drag by surface pressure integrations involves subtractive cancellation that may lead to a loss of accuracy.

An alternate approach is the far-field method which can determine the induced drag in the Trefftz plane without restriction to subsonic flow.

This series of lectures will address the following topics:

1. Derivation of formulae for far-field drag integration.

2. Trefftz plane integration of computational results.

3. Influence of wake shape on far-field drag computation.

4. Munk's stagger theorem.

5. Nonlinear considerations in the application of Munk's Stagger Theorem.

In the following derivations, care is taken to preserve u-perturbation terms that arise from the force-free wake, often neglected in traditional developments [1]. The influence of the wake shape on the Trefftz-plane integration is discussed, and a criterion is established for assessing the extent of force-free wake modeling required to capture the interaction of the wake with the wing.

These lecture notes have been compiled from Chapter 3 of Dr. Steve Smith's Ph.D. thesis [2].

Far-Field Drag Computation

Von Karman suggested that conservation principles could be applied to a control volume surrounding a finite wing to determine the induced drag, based on the residual flow perturbations exiting the volume in the vicinity of the wake

In the following development, an expression for the induced drag is derived from momentum conservation. The control volume is taken as fixed in the inertial reference frame of the wing, moving at the constant velocity, U_∞ with respect to the undisturbed fluid. The control volume and relevant nomenclature are shown in Figure 1. The lateral, top, and bottom surfaces of the volume are aligned parallel to the flight path, and the fore and aft surfaces are aligned perpendicular to the flight path. Additional bounding surfaces are coincident with the wing surface and the upper and lower surfaces of the trailing wake discontinuity. Surface unit-normal vectors are positive outward. For a finite wing, the interior volume is simply connected.

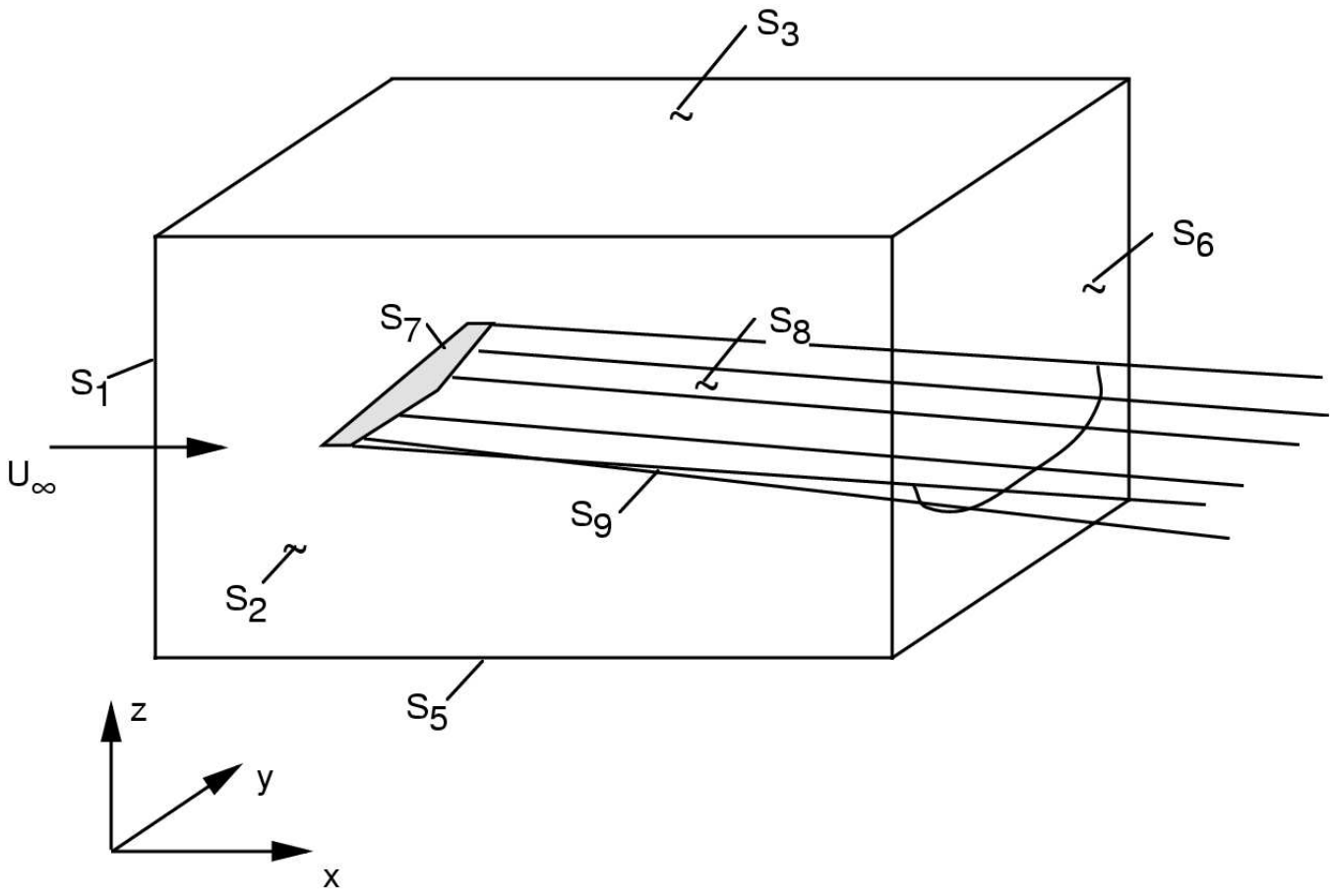

Figure 1: Control Volume for Momentum Conservation

In fact, Von Karman's analysis was incorrect. He chose a steady reference frame fixed to the wing. In this frame, there is no work done on the wing, since it doesn't move. The kinetic energy, $E = 1/2\rho \iint (u^2 + v^2 + w^2)\, ds$ simply balances the work done on the flow by the pressure on the boundaries. Von Karman's result matches the now-accepted expression for the drag only at the point of neglecting the longitudinal perturbation velocity. An energy balance in an unsteady, ground-fixed reference frame does produce an expression for the induced drag, but special care must be taken to correctly account for the unsteady potential terms. Shoemaker showed that this analysis leads to the same result as the more customary momentum balance in the steady reference frame:$D = 1/2\rho \iint (v^2 + w^2 - u^2)\, ds$ [3].

Conservation of Momentum Applied to a Finite Wing

In the absence of any forces, an expression for conservation of momentum in this volume is given by:

$$\frac{D\mathbf{P}}{Dt} = -\frac{d}{dt}\iiint \rho\mathbf{V}\,dv - \iint \rho\mathbf{V}(\mathbf{V}\cdot\hat{\mathbf{n}})\,ds = 0 \tag{1}$$

It is important to note here that the development of this Eulerian expression for momentum conservation requires that the velocity field be continuous. When any forces are present, Newton's second law requires

$$\mathbf{F} = \frac{D\mathbf{P}}{Dt} = -\frac{d}{dt}\iiint \rho\mathbf{V}\,dv - \iint \rho\mathbf{V}(\mathbf{V}\cdot\hat{\mathbf{n}})\,ds \tag{2}$$

For stationary flow, there can be no accumulation of momentum within the

volume, so

$$\mathbf{F} = -\iint \rho \mathbf{V}(\mathbf{V} \cdot \hat{\mathbf{n}})\, ds \tag{3}$$

For simplicity in this development, body forces are excluded. In addition, the flow is assumed to be inviscid, so surface shear stresses are neglected. The remaining surface force on the boundary is simply the surface integral of the pressure, so

$$\iint p\mathbf{n}\, ds = -\iint \rho \mathbf{V}(\mathbf{V} \cdot \hat{\mathbf{n}})\, ds \tag{4}$$

Since the purpose of this development is to derive an expression for the drag, only the x-component of the force and momentum, parallel to the freestream, will be considered:

$$\iint p n_x\, ds = -\iint \rho V_x(\mathbf{V} \cdot \hat{\mathbf{n}})\, ds \tag{5}$$

The contributions to these surface integrals from the various surfaces of the control volume can now be evaluated separately. The surfaces bounding the wake discontinuity, S_8 and S_9, are considered first. To evaluate these, we must make one of two assumptions about the wake. Either it is a truly force-free wake, aligned everywhere with the local flow, or it is a drag-free wake, aligned with the freestream. In the first case, there is no pressure differential across the wake, and $\mathbf{V} \cdot \hat{\mathbf{n}} = 0$ on the wake surfaces. The unit normals, $\hat{\mathbf{n}}_8$ and $\hat{\mathbf{n}}_9$ have opposite sign, so

$$\iint_8 p n_x \, ds + \iint_9 p n_x \, ds = 0 \quad \text{and} \iint_{8,9} \rho V_x (\mathbf{V} \cdot \hat{\mathbf{n}}) \, ds = 0 \qquad (6)$$

In the second case, a pressure differential may exist, but $n_x = 0$. There is a tangential velocity (V_y) discontinuity but V_x and V_z are continuous. Again,

$\mathbf{n}_8$ and $\mathbf{n}_9$ have opposite sign, so

$$\iint_{8,9} p n_x \, ds = 0 \quad \text{and} \iint_8 \rho V_x (\mathbf{V} \cdot \hat{\mathbf{n}}) \, ds + \iint_9 \rho V_x (\mathbf{V} \cdot \hat{\mathbf{n}}) \, ds = 0 \tag{7}$$

For both of the wake positions considered, the contribution of the wake-bounding surfaces to the x-component momentum balance is zero. Next consider the surface surrounding the wing, S_7. On the wing surface, $\mathbf{V} \cdot \hat{\mathbf{n}} = 0$, and the pressure integral is the drag:

$$\iint_7 p n_x \, ds = D \tag{8}$$

For an inviscid flow that is everywhere subsonic, this drag is defined as the induced drag, D_i. It will be shown that the induced drag is the result of the momentum left in the flow associated with the trailing wake vorticity. The

surfaces that remain constitute the six exterior faces of the control volume. Note that $n_x = 0$ on the top, bottom, and side faces, $n_x = -1$ on the front face, and $n_x = 1$ on the rear face. At this point, it is convenient to express the pressure and velocity in terms of perturbations from the freestream, so the drag expression becomes:

$$\begin{aligned} D_i \quad + \quad & \iint_6 (p - p_\infty)\, ds - \iint_1 (p - p_\infty)\, ds = \\ - \quad & \iint_3 \rho(U_\infty + u) w\, ds + \iint_5 \rho(U_\infty + u) w\, ds + \iint_2 \rho(U_\infty + u) v\, ds \\ - \quad & \iint_4 \rho(U_\infty + u) v\, ds + \iint_1 \rho(U_\infty + u)^2\, ds - \iint_6 \rho(U_\infty + u)^2\, ds \end{aligned} \tag{9}$$

For stationary flow through this volume, mass conservation is expressed by:

$$\iint \rho(\mathbf{V} \cdot \hat{\mathbf{n}})\, ds = 0 \tag{10}$$

Expressing this in terms of perturbations from the freestream gives:

$$\begin{aligned} \iint_3 \rho w\, ds \quad &- \quad \iint_5 \rho w\, ds - \iint_2 \rho v\, ds + \iint_4 \rho v\, ds \\ &- \quad \iint_1 \rho(U_\infty + u)\, ds + \iint_6 \rho(U_\infty + u)\, ds = 0 \end{aligned} \tag{11}$$

Substitution of this into equation 9 yields:

$$D_i + \iint_6 (p - p_\infty)\, ds - \iint_1 (p - p_\infty)\, ds = - \iint_3 \rho u w\, ds + \iint_5 \rho u w\, ds$$

$$+\iint_2 \rho uv\,ds - \iint_4 \rho uv\,ds + \iint_1 \rho u(U_\infty + u)\,ds - \iint_6 \rho u(U_\infty + u)\,ds \quad (12)$$

As the control volume size is increased, the perturbation velocities on the front, top, bottom, and side faces become diminishingly small, leaving, eliminating higher order terms:

$$D_i = -\iint_6 (p - p_\infty)\,ds - \iint_6 \rho u(U_\infty + u)\,ds \quad (13)$$

At this point, a relationship between the pressure and velocity on surface S_6 is needed. Rather than restrict this development to incompressible flow, the compressible form of Bernoulli's equation will be used. However, the flow through surface S_6 is regarded as a small perturbation from the freestream, caused only by the induced velocities from the trailing wake. For any subsonic freestream Mach number, the cross-flow perturbations are

small compared to the speed of sound. Assuming small perturbations and isentropic flow, a second-order accurate form of Bernoulli's equation is given by:

$$p - p_\infty = -\frac{1}{2}\rho_\infty \left\{ 2uU_\infty + (1 - M_\infty^2)u^2 + v^2 + w^2 \right\} \tag{14}$$

The derivation of this form of Bernoulli's equation can be found in the Appendix of reference [2]. Substituting this relation, the drag equation becomes:

$$D_i = \frac{1}{2}\rho_\infty \iint_6 \left\{ 2uU_\infty + (1 - M_\infty^2)u^2 + v^2 + w^2 \right\} ds - \iint_6 \rho u(U_\infty + u)\, ds \tag{15}$$

The density in the second integral may also be expressed as a perturbation from freestream, $\rho = \rho_\infty + \rho'$. Substituting and collecting terms,

$$D_i = \frac{1}{2}\rho_\infty \iint_6 (v^2 + w^2 + u^2)\, ds - U_\infty \iint_6 \rho' u\, ds$$

$$- \iint_6 \rho' u^2 \, ds - \frac{1}{2}\rho_\infty (2 + M_\infty^2) \iint_6 u^2 \, ds \tag{16}$$

The derivation of a second-order accurate expression for the perturbation density, ρ', follows the derivation for Bernoulli's equation, producing:

$$\rho' = -\frac{1}{2}\rho_\infty \frac{M_\infty^2}{U_\infty^2} \left\{ 2uU_\infty + \left(1 - (2-\gamma)M_\infty^2\right) u^2 + v^2 + w^2 \right\} \tag{17}$$

Substituting this into Equation 16 and collecting terms:

$$\begin{aligned} D_i &= \frac{1}{2}\rho_\infty \iint_6 \left\{ (v^2 + w^2 + u^2) + (M_\infty^2 - 2)u^2 \right. \\ &\quad \left. + \frac{M_\infty^2 u}{U_\infty} \left((\gamma - 2) M_\infty^2 u^2 + v^2 + w^2 \right) \right\} ds \end{aligned} \tag{18}$$

This expression relates the induced drag to the perturbation velocities in a transverse plane defined by the rear face of the control volume. With the assumptions already made, (i.e. inviscid, isentropic flow) potential flow exists outside the wake, so that

$$\begin{aligned} \iint (v^2 + w^2 + u^2)\, ds &= \iint \left\{ \left(\frac{\partial \phi}{\partial x}\right)^2 + \left(\frac{\partial \phi}{\partial y}\right)^2 + \left(\frac{\partial \phi}{\partial z}\right)^2 \right\} ds \\ &= \iint \nabla\phi \cdot \nabla\phi \, ds \end{aligned} \tag{19}$$

The vector identity $\nabla\phi \cdot \nabla\phi = \nabla \cdot \phi\nabla\phi - \phi\nabla^2\phi$ may be substituted, noting that $\nabla^2\phi = 0$ outside the wake:

$$\iint (v^2 + w^2 + u^2)\, ds = \iint \nabla \cdot \phi\nabla\phi \, ds \tag{20}$$

Separating the divergence term into cross flow and freestream components,

$$\begin{aligned}\iint \nabla \cdot \phi \nabla \phi \, ds &= \iint \left\{ (\nabla \cdot \phi \nabla \phi)_{yz} + \frac{\partial}{\partial x}\left(\phi \frac{\partial \phi}{\partial x} \right) \right\} ds \\ &= \iint \left\{ (\nabla \cdot \phi \nabla \phi)_{yz} + \phi \frac{\partial u}{\partial x} + u^2 \right\} ds \end{aligned} \quad (21)$$

Gauss' theorem relates the area integral of the two dimensional divergence to a contour integral on the boundary. In this case, the boundary includes a contour surrounding the trace of the wake discontinuity on the surface, S_6. In general,

$$\iint \nabla \cdot \mathbf{F} \, ds = \oint \mathbf{F} \cdot \hat{\mathbf{n}} \, dl \quad (22)$$

so,

$$\iint \nabla \cdot \phi \nabla \phi \, ds = \oint \phi (\nabla \phi \cdot \hat{\mathbf{n}}) \, dl = \oint \phi \left(\frac{\partial \phi}{\partial n} \right) dl \quad (23)$$

Substituting these relations into Equation 18 gives:

$$D_i = \frac{1}{2}\rho_\infty \int_{-L}^{L} \Delta\phi \left(\frac{\partial \phi}{\partial n}\right) dl + \frac{1}{2}\rho_\infty \iint_6 \left\{ \phi \frac{\partial u}{\partial x} + (M_\infty^2 - 1)u^2 + \frac{M_\infty^2 u}{U_\infty}\left((\gamma - 2)M_\infty^2 u^2 + v^2 + w^2 \right) \right\} ds \quad (24)$$

where the contour integral has been replaced by a simple line integral along the wake trace from tip to tip. $\Delta\phi$ is the potential jump from the upper side to the lower side of the wake. Note that although the potential is discontinuous across the wake, the normal velocity, $\frac{\partial \phi}{\partial n}$ is continuous. The remaining surface integral depends only the u-perturbation velocity and its streamwise gradient. When the rear surface of the control volume is moved far downstream of the lifting system, the u-perturbation produced by the bound vorticity becomes diminishingly small, leaving only the perturbations

produced by the trailing wake. This surface is traditionally referred to as the Trefftz plane. For the case of the streamwise wake, the wake cannot produce any u-perturbation, and the induced drag becomes simply:

$$D_i = \frac{1}{2}\rho_\infty \int_{-L}^{L} \Delta\phi \left(\frac{\partial \phi}{\partial n}\right) dl \tag{25}$$

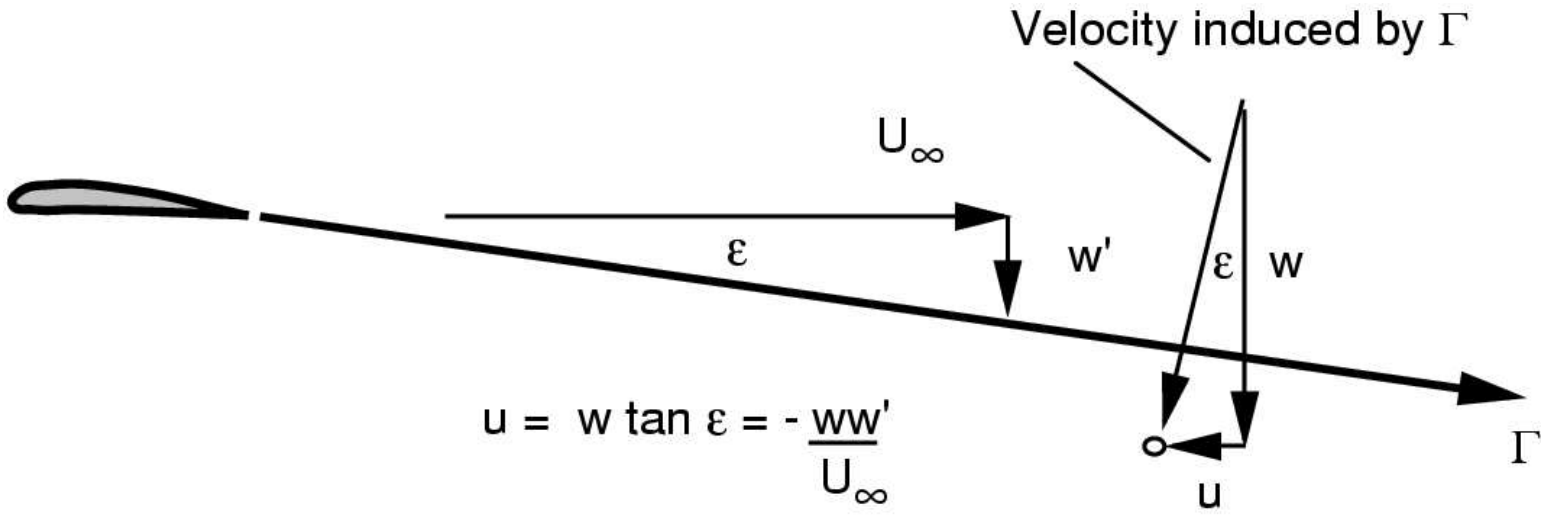

Figure 2: U-Perturbation Produced When Wake is Not Aligned with Freestream

For the force-free wake, u-perturbations are produced in the Trefftz plane because the vorticity is not perpendicular to the plane. Where a portion of wake is displaced by an angle $\varepsilon = -w'/U_\infty$, as shown in Figure 2, the

induced velocity has a u component, related to the w component by

$$u = w \, \tan \varepsilon = -w \, w'/U_\infty .$$

Here, w' is the induced velocity on the wake and w is the z-component of the velocity induced by the vortex. The u^2 and uw^2 terms in the surface integral are $O(w^4)$, and uv^2 is $O(v^4)$, whereas the dominant terms of Equation 18 are of order $O(w^2 + v^2)$. Traditionally, these higher-order terms are neglected based on the assumptions that the wake deflection is small and the perturbations are small compared with the freestream velocity. The $\frac{\partial u}{\partial x}$ term arises from the curvature and nonparallel nature of the vortices in the deformed wake. However, for typical wings, the wake shape is observed to evolve only slowly, so the $\frac{\partial u}{\partial x}$ term is also traditionally neglected.

If the induced drag must be computed with sufficient accuracy to resolve small differences (as is the case in design optimization studies,

where improvements sought may be only 1–2% of the drag) one must be careful in eliminating some of these terms. In Chapter 6 of reference [2], the magnitudes of these higher-order terms are numerically evaluated for a typical force-free wake to confirm that their contribution is negligibly small. Once this is done, the line integral in Equation 25 can be used to evaluate the induced drag on a force-free wake. The Trefftz-plane line integral, Equation 25, provides a simple means to evaluate the induced drag in the far-field from computational results. The potential jump and normal velocity may be surveyed and numerically integrated along the wake trace. It is worthwhile to restate the assumptions employed to derive this Trefftz-plane drag integral here:

1. The flow is assumed to be continuous, stationary, and inviscid.

2. The trailing wake is either force-free, or drag-free by virtue of trailing in the freestream direction. This does not imply that the two different

wake shapes would produce the same drag, only that the derivation is valid in both cases.

3. The flow is isentropic, perfect gas, and in the vicinity of the wake far away from the wing, may be considered as a small perturbation from the freestream.

4. The force-free wake evolution is slow enough that u-perturbations are assumed to be negligible; the flow can be considered two dimensional in the Trefftz plane.

This derivation puts no explicit limitation on Mach number, although the requirement that the flow be continuous restricts straightforward application to Mach numbers less than 1.0. The appearance of shocks in the flow creates a problem, since they represent discontinuities in potential flow. The jump conditions that exist across the shock discontinuity are dependent on the

specific governing equations used to describe the flow. Since the scope of these lectures involves drag predictions in potential flow, the isentropic shock jump conditions produced by the weak solution of the full potential equation will be considered. The control volume used to express momentum conservation must be modified from the previous development because of the presence of the shocks. As shown in Figure 3, additional bounding surfaces, S_{10} and S_{11}, surround the shock.

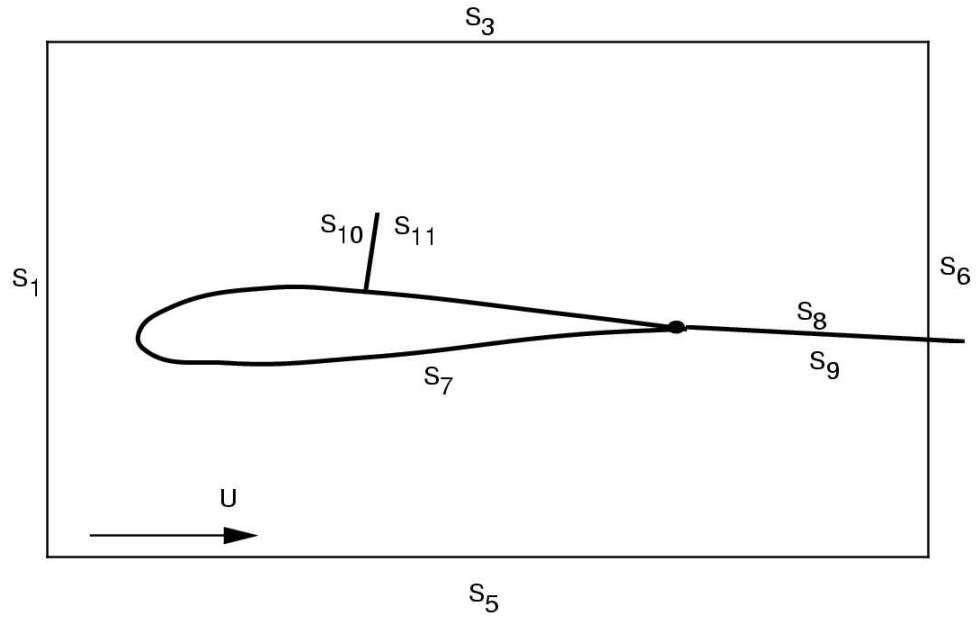

Figure 3: Additional Bounding Surfaces on Shock Discontinuity

The domain inclosed by the new control volume is still simply connected. After expanding the control volume large enough to eliminate the contributions on the forward and side faces, the expression for the drag

becomes:

$$D = D_i + D_w = -\iint_6 (p - p_\infty)\, ds - \iint_6 \rho u (U_\infty + u)\, ds - \iint_{10} p n_x\, ds$$
$$- \iint_{10} \rho (U_\infty + u)(\mathbf{V} \cdot \hat{\mathbf{n}})\, ds - \iint_{11} p n_x\, ds - \iint_{11} \rho (U_\infty + u)(\mathbf{V} \cdot \hat{\mathbf{n}})\, ds \quad (26)$$

where the drag now includes the wave drag. Since surfaces S_{10} and S_{11} are identical except for the direction of the normal, these integrals can be combined so that:

$$D_i + D_w = -\iint_6 (p - p_\infty)\, ds - \iint_6 \rho u (U_\infty + u)\, ds$$
$$- \iint_{10} \left\{ (p_{10} - p_{11}) n_x + \rho u (\mathbf{V} \cdot \hat{\mathbf{n}})_{10} - \rho u_{11} (\mathbf{V}_{11} \cdot \hat{\mathbf{n}}_{10}) \right\} ds$$

$$- U_\infty \iint_{10} \left\{ \rho(\mathbf{V} \cdot \hat{\mathbf{n}})_{10} - \rho(\mathbf{V}_{11} \cdot \hat{\mathbf{n}}_{10}) \right\} ds \tag{27}$$

The last integral is zero based on mass conservation across the shock. Mass conservation is satisfied by both the isentropic shock and the Rankine-Hugoniot shock jump relations. The drag becomes:

$$\begin{aligned} D_i \quad + \quad D_w = & - \iint_6 (p - p_\infty)\, ds - \iint_6 \rho u (U_\infty + u)\, ds \\ & - \iint_{10} \left\{ (p_{10} - p_{11}) n_{x10} + \rho u (\mathbf{V} \cdot \hat{\mathbf{n}})_{10} - \rho u_{11} (\mathbf{V}_{11} \cdot \hat{\mathbf{n}}_{10}) \right\} ds \end{aligned} \tag{28}$$

The remaining integral on the shock surface represents the normal-momentum change across the shock. Note that the Rankine-Hugoniot

shock relations explicitly conserve the normal-momentum across the shock,

$$(p_{10} - p_{11})n_{x10} + \rho u_{10}(\mathbf{V} \cdot \hat{\mathbf{n}})_{10} - \rho u_{11}(\mathbf{V}_{11} \cdot \hat{\mathbf{n}}_{10}) = 0 \qquad (29)$$

so the integral on the shock surface is zero. This leaves only the Trefftz plane integral on S_6 to capture both the induced drag and the wave drag. In an inviscid, rotational flow, the loss of total pressure across the shock becomes the mechanism for convecting the wave drag downstream to the Trefftz plane. In this case, the shock surface added to the control volume appears unnecessary; no discontinuity in momentum occurs and the same integral relation results in either case.

In the case of potential flow, the isentropic shock jump relations do not conserve the normal-component of momentum, so the integral over the shock surface is finite. On the other hand, the total pressure is constant in the Trefftz plane, equal to the freestream value. Also, in the absence of the

wake vorticity in the far field, the perturbation potential in the Trefftz plane must decay to zero; the Trefftz-plane drag vanishes. Evidently, in potential flow only the induced drag appears in the far-field integral, and the wave drag is in equilibrium with the normal-momentum jump across the shock surface. This assertion has been widely discussed by Steger and Baldwin, Henne and Hicks, van der Vooren and Sloof, among others, [4, 5, 6]. The expression for the induced drag in transonic potential flow is identical to Equation 13, and the remaining development leading to Equation 25 is the same.

Trefftz-Plane Integration of Computational Results

When computational methods such as the A502 panel code or the Tranair full-potential code are used to analyze wings, the induced drag may be determined by the Trefftz-plane integration method developed earlier, provided the required wake properties can be obtained as outputs from the computational method. Both A502 and Tranair provide an off-body flow survey as an output feature. At specified points in the flow off the surface of the geometry, the three components of velocity and the perturbation potential are output. The user may specify that the contribution of some portion of the geometry to these properties be excluded from the survey.

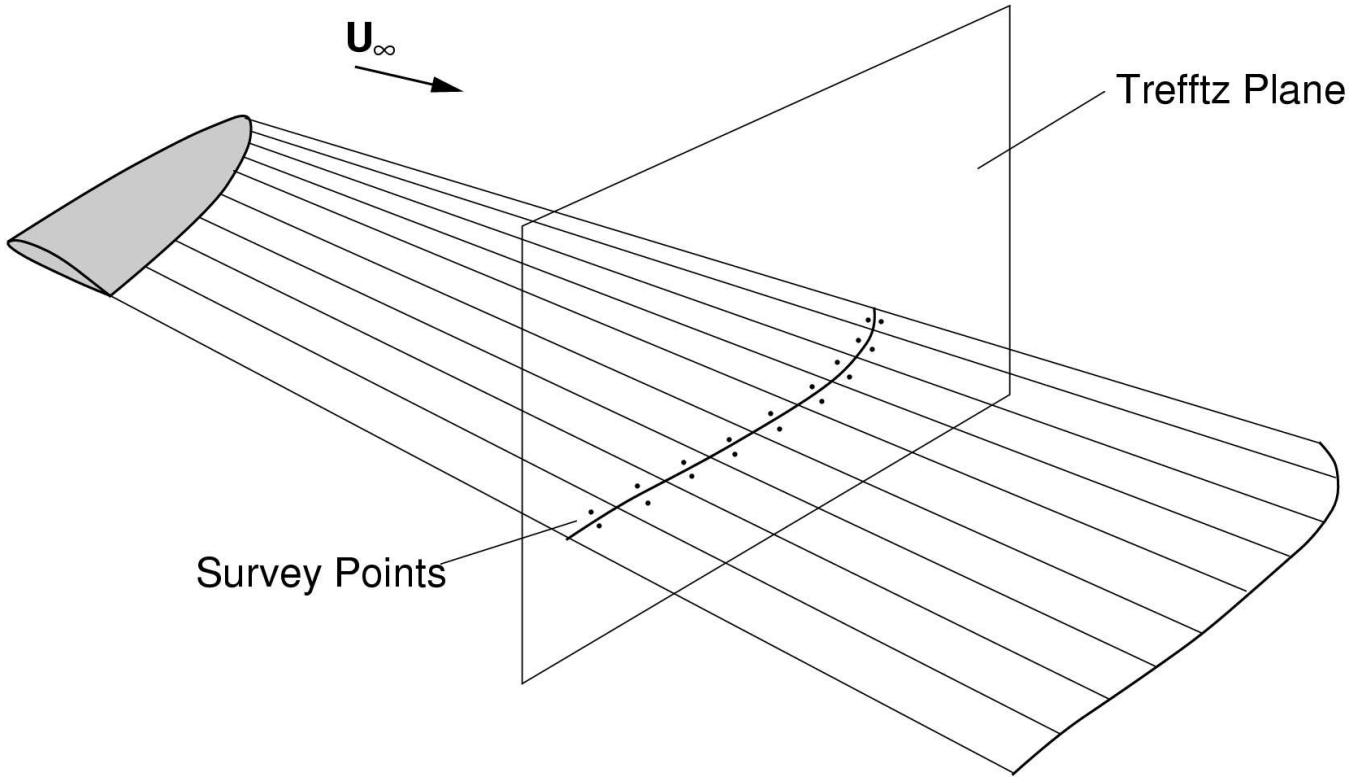

Figure 4: Survey Points Used to Determine Wake Properties in Trefftz Plane

To measure the wake properties needed for Trefftz-plane integration,

pairs of survey points are located along the wake a very small distance above and below the wake, shown in Figure 4. The survey must be made far enough downstream of the lifting system so that the assumptions leading to Equation 25 are valid. The wake model must also be extended a considerable distance downstream of the survey so that the velocities induced are representative of an infinite wake.

Typically, for accurate drag calculations, the wake is extended 30 semispans downstream of the trailing edge, and the Trefftz plane survey is located 15 semispans downstream of the trailing edge. The A502 high-order panel code, or the Tranair full-potential code can be used to compute the velocity and perturbation potential at these points. The velocity in the wake at a particular station is found by averaging the velocities of the corresponding pair of survey points, and the jump in potential across the wake is found by the difference in potential between the two points. These results are then integrated numerically using the trapezoidal rule.

Influence of Wake Shape on Far-Field Drag Computation

The far-field integral expression for the induced drag has been derived for the cases of a streamwise wake and a force-free wake. The consequence of any other wake shape is that the contribution of the wake-bounding surfaces, S_8 and S_9, to the force computation is non-zero. In other words, the drag (or thrust) on the wake shows up in the far-field integration. A pathological example of this is a wake which folds onto itself in the plane of symmetry, as shown in Figure 5. Here, the vorticity on the two halves of the wake cancel and the Trefftz-plane drag is zero. While this shape is rather non-physical, so is the commonly used streamwise wake.

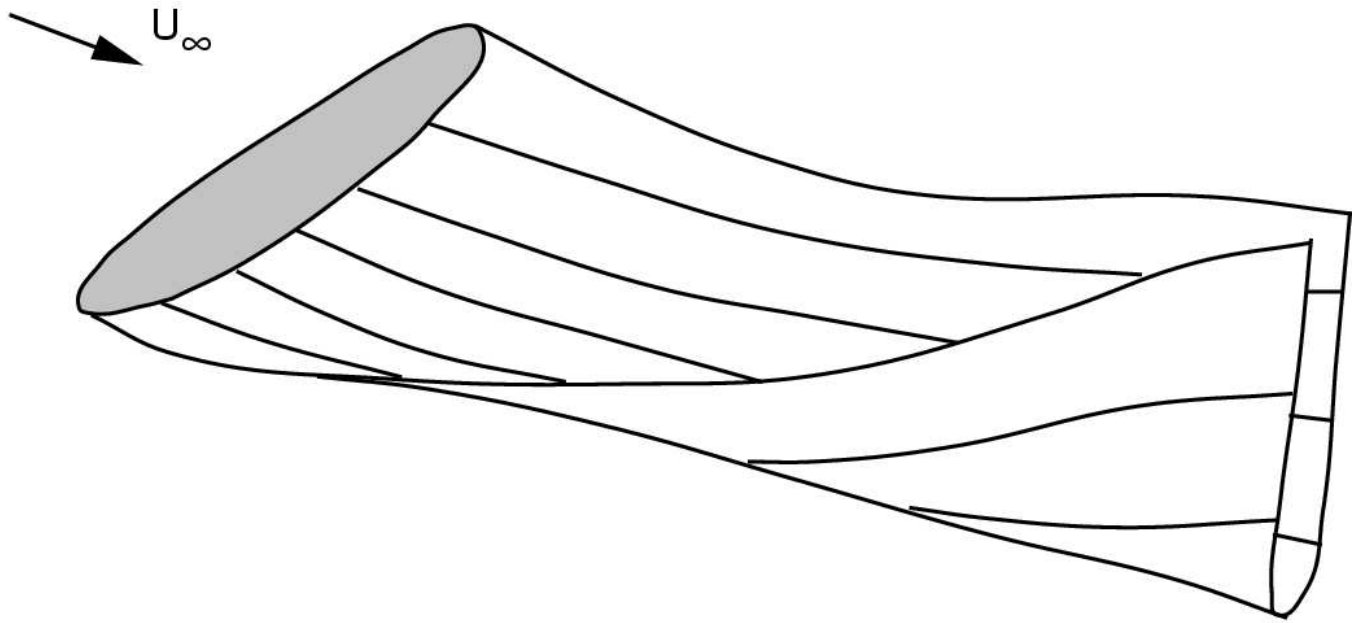

Figure 5: Non-physical Wake Shape with Zero Drag

It is not sufficient to argue that the wake deforms only slowly, and that the deformation has little effect on the downwash induced on the wing, as may be argued in the case of surface pressure integration. For the force-free wake, there is a small contribution to the drag from u-perturbation

velocities produced by the wake, given in Equation 24. For simplicity, only the case of low Mach number is considered here. For low speed flows, the u-perturbation contribution is:

$$\frac{1}{2}\rho_\infty \iint_6 \left(\phi \frac{\partial u}{\partial x} - u^2 \right) ds \tag{30}$$

As shown earlier, these terms are of $O(w^4)$, and are traditionally neglected in the far field where the contribution from the bound vorticity has died out. The magnitude of these terms for a typical wake are evaluated numerically in Chapter 6 of reference [2]. The benefit of neglecting these terms is that the expression for the induced drag reduces to the simple line integral in Equation 25, The same expression is exact for the streamwise wake model. However, the question of whether the induced drag computed from the streamwise wake model is the same as the drag computed from a force-free wake model remains. This question actually has two parts. First, if the

circulation distribution shed into the wake is fixed, is the Trefftz-plane drag affected by the wake shape, and secondly, is the circulation distribution affected? The first question may be addressed by introducing a partition surface into the control volume, in between the wing and the Trefftz plane. This partition is illustrated in Figure 6. The arrangement of the control volumes resulting from this partition is shown in Figure 7. The forward, side, top, and bottom faces of the near-field control volume are still moved far away, so the induced drag within the near-field volume may be evaluated by a surface integral on the partition using Equation 18 simplified here for low Mach number:

$$D_i = \frac{1}{2}\rho_\infty \iint_P \left(v^2 + w^2 - u^2 \right) ds \tag{31}$$

where the subscript P denotes the partition surface. Note that this integral is not restricted by the far-field assumption that the influence of the wing has died out.

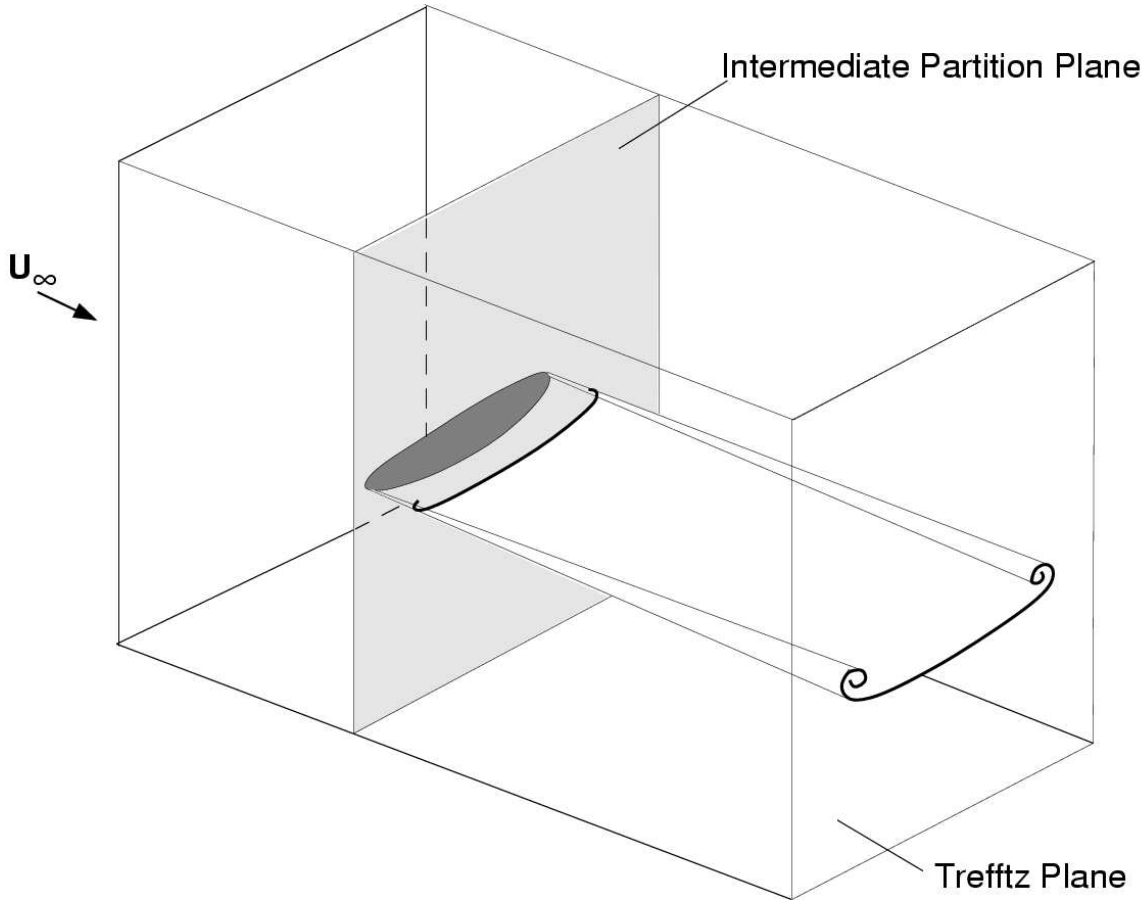

Figure 6: Intermediate Partition in Control Volume

The induced drag within the entire far-field control volume is still given by Equation 24. Provided that the wake is drag-free, the induced drag within the wake control volume is zero. It follows that the two drag computations must agree. Now, the portion of the force-free wake downstream of the partition may be replaced with a drag-free wake constructed as a freestream projection of the trace of the wake on the intermediate partition.

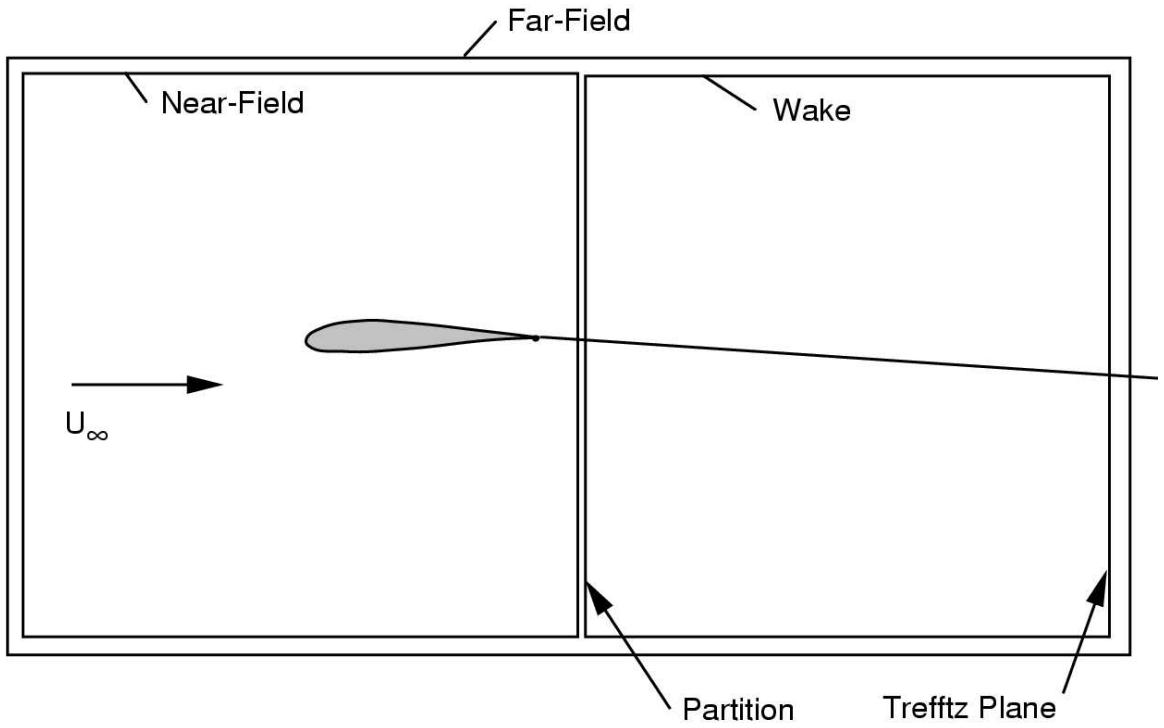

Figure 7: Near-Field and Wake Control Volumes

The drag computed on the two planes will still agree. Of course, this does not preclude that both results may change. The wake substitution

changes the perturbation velocities induced on the partition surface by the wake by changing the deflection angle of half the wake with respect to the partition. This removes approximately half the u-perturbation. Perhaps more important, the wake substitution also increases the effective distance between a vortex filament and a point in the plane, reducing the induced v and w perturbations, as shown in Figure 8. If a wake filament has little or no curvature, the reduction of induced velocity is proportional to the cosine of the deflection angle.

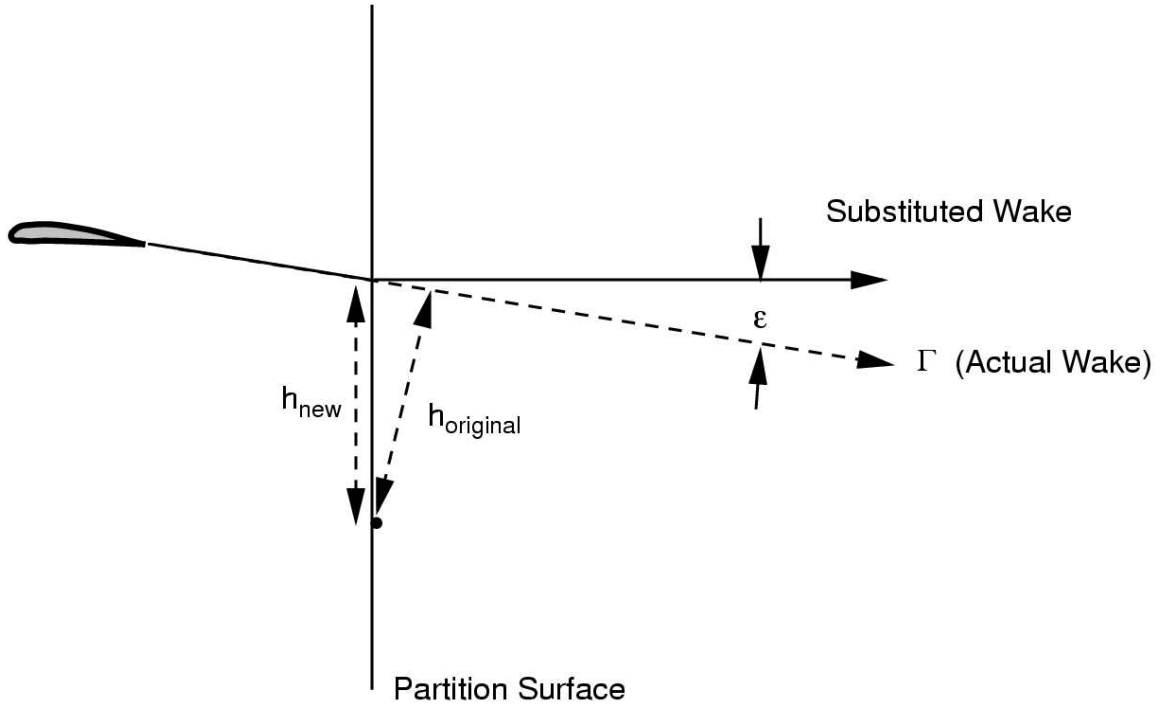

Figure 8: Wake Substitution Modifies Induced Velocities

However, if the vortex curvature is significant, the modification of the induced velocity field in the partition may be more pronounced. As

mentioned before, the wake deforms slowly for typical wings, so these effects are expected to be small. This allows substitution of a streamwise wake downstream of the partition with only small error. The need for high-accuracy drag prediction for drag minimization studies requires that the magnitude of these effects be quantified. In Chapter 6 of reference [2], the change in drag computed in the Trefftz plane produced by streamwise wake substitution is investigated numerically for two typical planar wings. Those results confirm that the error is negligible, even for the requirements of this study. For typical wing planforms, the deflection angle and curvature of the individual vortex filaments do not vary significantly along the length of the wake, so these small errors do not increase with proximity of the substitution point to the lifting system. The additional u-perturbation induced by the bound vorticity on the wing is not affected by the wake substitution. Therefore, the streamwise wake substitution may be made immediately downstream of the lifting system, as long as the above assumptions are valid. There may be cases where the wake deforms rapidly for a short

distance downstream of the wing. In these cases, the high wake curvature may introduce some error, and the wake substitution should be delayed for a short distance downstream. As the partition where the streamwise wake substitution is made is brought close to the downstream extremity of the lifting system, most of the force-free wake and its influence on the wing planform is removed. In the special case of a wing with an unswept trailing edge, all of the wake may be replaced. In other cases, a small portion of force-free wake remains, as shown in Figure 9.

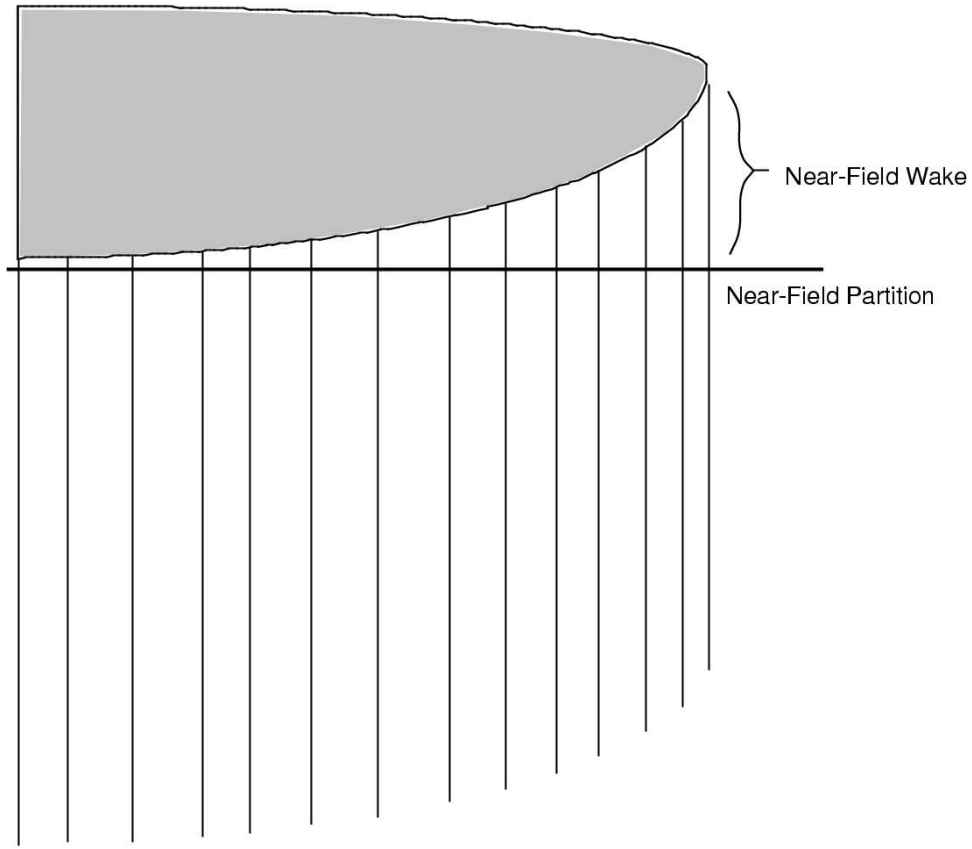

Figure 9: Near-Field Portion of Force-Free Wake Remains After Substitution

At this point, one may be tempted to extend the process of wake substitution further by arguing that the intermediate partition need not be perpendicular to the freestream. In particular, it might be arranged to match the trailing edge sweep of the wing, allowing more of the force-free wake to be eliminated. The full application of this argument, after all, leads to the traditional streamwise wake model where all of the force-free wake is substituted. However, when this is done, the changes in perturbation velocities induced on the partition surface are no longer negligible. Equation 31 must be re-cast to account for the orientation of the partition. In the following example, the partition is rotated by an angle λ about the z-axis. Since the purpose of the rotation is to match a trailing edge sweep angle, λ is not considered small. The revised expression for the induced drag on P is:

$$D_i = \frac{1}{2}\rho_\infty \iint_p \left(v^2 + w^2 - u^2 \right) \cos\lambda \, ds$$

$$+ \rho_\infty \iint_p uv \sin\lambda \, ds \tag{32}$$

For a two dimensional (infinite) wake, the second integral is zero since the u- perturbation contributed by each individual vortex filament is an odd function of y centered about the filament, and the v-perturbation is an odd function of z centered about the filament. By superposition, this term would integrate to zero. However, because the wake is not two dimensional and the surface is swept, the distributions of u and v on the partition surface induced by each filament are not symmetrical. This becomes more pronounced as the surface is moved to proximity with the wing trailing edge, where the wake appears semi-infinite. Further, although u^2 is $O(w^4)$ as before, the uv term is $O(w^3)$. When the substitution of the streamwise wake is made, approximately half the contribution of the uv-perturbation is removed. Even for a modest sweep angle λ, this error is greater than the error produced by the more restrictive case where

the partition is perpendicular to the freestream. Planforms with forward sweep in the trailing edge such as shown in Figure 9 result in strong wake vorticity being shed well ahead of the partition. Based on the preceding discussion, the replacement of the initial roll-up region of the wake with a streamwise wake cannot be performed without substantially influencing the Trefftz-plane drag. The presence of this remaining portion of force-free wake represents the potential for wake interactions that would be overlooked by the traditional engineering approach. This wake interaction is discussed further in the following section. There is still the remaining question of whether the wake substitution modifies the distribution of bound circulation on the wing. Evidence suggests that the presence of the force-free near wake does modify the circulation distribution slightly from the solution with the classical streamwise wake [7]. In any case, the numerical examples in Chapter 6 of reference [2] quantify the errors resulting from wake substitution, including the effect of any change in circulation distribution.

Nonlinear Considerations in the Application of Munk's Stagger Theorem

Munk's stagger theorem [8], that the induced drag of a lifting system is determined only by the wake shape and the vorticity distribution in the wake, follows from earlier derivations. However, our derivations required that the wake must be either the true force-free shape, or a drag-free streamwise wake. Munk's condition for minimum induced drag for nonplanar wakes is that the "normalwash" in the Trefftz plane is proportional to the cosine of the local dihedral angle.

$$\mathbf{V} \cdot \hat{\mathbf{n}} = w_o \cos\beta \tag{33}$$

Attempting to minimize drag by applying this condition on the force-free wake would be difficult, since it would be practically impossible to design the wing that would produce a specific wake shape and vorticity distribution. However, minimizing drag of wings with streamwise wakes has been done extensively by Cone [9], Lowson [10], and others. Burkett and

Lowson observed that the wake shape is altered by a coupling between the longitudinal arrangement of vortex elements on the wing and the angle of attack [11, 10]. Since all the vorticity sheds from the trailing edge, the projection of the trailing edge onto the Trefftz plane determines the wake shape. The often-stated consequence of the stagger theorem, that the longitudinal arrangement of vortex elements does not affect the drag, must be reconsidered. A planar wing may create a nonplanar wake, as shown in Figure 10.

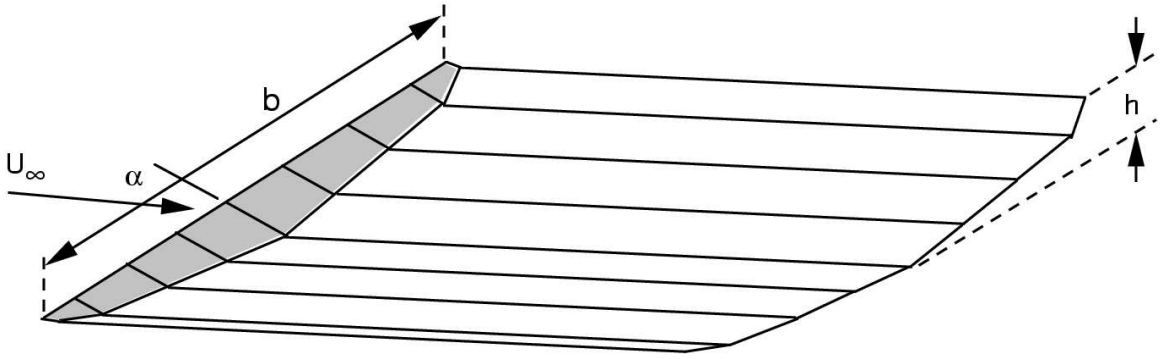

Figure 10: Planar Wing Producing a Nonplanar Wake

This influence of the trailing edge shape on the wake shape is still within the linear theory. The conclusions of earlier slides suggest additional, nonlinear influence of the longitudinal stagger (planform shape) on the wake shape. The streamwise wake substitution can only extend to the point where the partition intersects the downstream extremity of the lifting system. In essence, it is the shape of the force- free wake at this near-field partition that influences the far-field drag. Planforms with a significant portion of force-free wake remaining between the trailing edge and the partition have the greatest potential for favorable wake interference by creating a highly nonplanar wake. Two planar wing designs which attempt to exploit the benefit of a nonplanar wake are studied in Chapter 7 of reference [2].

References

[1] D. Kuchemann. *The Aerodynamic Design of Aircraft*. Pergamon Press,

1978.

[2] S. C. Smith. *A Computational and Experimental Study of Nonlinear Aspects of Induced Drag*. Ph.D. Dissertation, Department of Aeronautics and Astronautics, Stanford University, Stanford, CA, June 1995.

[3] W. C. Shoemaker. *A Wake Integral Method for Experimental Drag Measurement and Decomposition*. Ph.D. Dissertation, Department of Aeronautics and Astronautics, Stanford University, Stanford, CA, August 1994.

[4] J. L. Steger and B. S. Baldwin. Shock waves and drag in the numerical calculation of isentropic transonic flow. NASA TN D-6997, October 1972.

[5] P. A. Henne and R. M. Hicks. Wing analysis using a transonic potential flow computational method. NASA TM 78464, 1978.

[6] J. van der Vooren and J. W. Sloof. Cfd-based drag prediction; state-of-the- art, theory, prospects. TP 90247 L, NLR, 1990.

[7] I. M. Kroo and S. C. Smith. Computation of induced drag with nonplanar and deformed wakes. In *SAE Aerotech-90*, Long Beach, CA, September 1990. $SAE\ Transactions$, SAE Paper 901933.

[8] M. M. Munk. The minimum induced drag of aerofoils. NACA Report 121, 1921.

[9] C. D. Cone. The theory of induced lift and minimum induced drag of nonplanar lifting systems. NASA TR R-139, 1962.

[10] M. V. Lowson. Minimum induced drag for wings with spanwise camber. *Journal of Aircraft*, 27(7):627–631, July 1990.

[11] C. W. Burkett. Reductions in induced drag of wings with highly swept and tapered wing tips. *Aeronautical Journal*, 93:400–405, December 1989.